Springer

Acta Mechanica Sinica

CrossMark click for updates

• RESEARCH PAPER •

Acta Mech. Sin., Vol. 39, 322347 (2023)
https://doi.org/10.1007/s10409-022-22347-x

Capillary phenomena in the corner of truncated-cone-shaped containers under microgravity

Shangtong Chen[1†], Chu Zhang[2,3†], Wen Li[1*], Yong Li[1], Fenglin Ding[1], and Qi Kang[2,3]

[1] *Beijing Institute of Control Engineering, China Academy of Space Technology, Beijing 100094, China;*
[2] *Institute of Mechanics, Chinese Academy of Sciences, Beijing 100190, China;*
[3] *College of Engineering and Science, University of Chinese Academy of Sciences, Beijing 100049, China*

Received September 8, 2022; accepted September 9, 2022; published online September 28, 2022

In the microgravity environment, liquid is usually adsorbed in corners or slots. Liquid accumulated in these regions is difficult to be removed and used. A mathematical model describing static profiles of the liquid accumulated in the corner of truncated-cone-shaped containers under microgravity is obtained through theoretical derivation in this paper. The profiles have two cases according to liquid's wettability and the angle of containers' corners. Once coordinates of an endpoint of the profile are known, the profile and volume of the liquid can be obtained using the Shooting method according to the mathematical model. Besides, if abscissa values of the endpoints are unknown, the profile of the liquid can also be obtained using the dichotomy method and shooting method when liquid volume is given. It is easier to use these methods than others proposed before and they can also be used to predict liquid's profiles in other conditions. Numerical simulation is performed with the volume of fluid method and the results are in good agreement with theoretical ones. Based on the mathematical model, the profile and volume of the liquid accumulated in the corner can be predicted accurately.

Capillary phenomena, Truncated-cone-shaped containers, Microgravity, Shooting method

Citation: S. Chen, C. Zhang, W. Li, Y. Li, F. Ding, and Q. Kang, Capillary phenomena in the corner of truncated-cone-shaped containers under microgravity, Acta Mech. Sin. **39**, 322347 (2023), https://doi.org/10.1007/s10409-022-22347-x

1. Introduction

In the microgravity environment, surface tension plays a dominant role so that liquid is usually adsorbed in corners or slots. Liquid containers, such as satellite propellant tanks, have a structure that consists of corners, reservoirs, etc. Liquid accumulated in these regions is difficult to be removed and used, which is a waste of precious liquid used on satellites. Therefore, it is of great significance to study liquid behaviour in corners of truncated-cone-shaped containers under microgravity.

Capillary phenomena in both static and dynamic states have been widely studied. The well-known Lucus-Washburn equation was derived by adopting a balance between the capillary driven force, the friction force on tube wall and the gravity force [1,2]. A second order differential equation was derived with consideration of the pressure loss at the tube entrance by Levine et al. [3]. Capillary driven flow in cylindrical tubes was divided into three regions by Stange et al. [4]. Chen et al. [5] studied capillary flow in oval tubes and proposed a new flow model in which capillary driven flow was divided into two regions. Dynamic equations of capillary driven flow in tubes with varying cross section [6,7], concentric annuli [8], axisymmetric geometries [9], complex containers [10], rectangular microchannel [11] and capillary tubes [12] were also derived. Dreyer et al. [13] studied capillary rise between parallel plates and Chen et al. [14] explored capillary flow between plates with varying cross-section. Dynamics in closed and open capillaries was studied by Ramakrishnan et al. [15]. The governing equation of capillary driven flow in interior corners was firstly derived by Weislogel and Lichter [16], and was extended to

†These authors contributed equally to this work.
*Corresponding author. E-mail address: gradylee@126.com (Wen Li)
Executive Editor: Chao Sun

corners formed by plates with varying wettability [17], rounded interior corners [18], corners formed by a plate and a rounded wall [19], curved interior corners [20], Taylor rising [21], small corners between two curved walls [22] and symmetric draining from corners [23]. Theories of capillary driven flows and drop tower experiments are adopted to analyze liquid behaviour in tanks under microgravity and optimize propellant management device of tanks [24,25].

Static free surfaces under microgravity also attracted much attention. Capillary free surfaces in containers and corners were analyzed and the Concus-Finn condition was proposed [26]. Carroll [27] derived theoretical expressions for profiles of liquid drops on cylindrical fibers. Michielsen et al. [28] studied liquid drops on conical fibers and obtained the final location and profiles of liquid drops through analyzing Gibbs free energy. Profiles of liquid drops at the tips of cylindrical fibers and at the bottom of cylindrical fibers standing on flat substrates were studied by Du et al. [29,30]. Liquid bridges between solid walls were comprehensively studied and their profiles were obtained [31-37]. Capillary surfaces in cubes [38] and polyhedral containers [39] were also discussed. The hydrodynamic stability of constrained capillary surfaces was comprehensively analyzed by Bostwick and Steen [40]. Capillary breakup of armored liquid filaments was explored by Zou et al. [41].

However, profiles of the liquid accumulated in corners of truncated-cone-shaped containers at equilibrium have not been studied yet. This study focuses on this problem and proposes a mathematical model to describe the profile. The theoretical derivation of the mathematical model is presented in this paper. Numerical simulation is performed with the volume of fluid (VOF) method by considering different liquid wettability, different volumes of liquid and different geometries of containers. Besides, a numerical method based on the shooting method is developed to predict profiles of the liquid accumulated in corners. Two situations are discussed. In the first case, the container's geometry, the liquid contact angle and the abscissa value of a point on the profile curve are known. In the second case, the container's geometry, the liquid contact angle and the volume of liquid are known. In previous study of liquid drops on conical fibers, the Gibbs free energy minimization method is adopted to calculate the profile in the second case, which is more complicated than the method proposed in this paper.

2. Theory

Liquid tanks in satellites are basically spherical or cylindrical and, in the microgravity environment, liquid is usually adsorbed in corners. When the amount of liquid is just enough, it will form a liquid ring covering the entire circle of the corner. And the profiles of liquid on all cross-sections are same. As shown in Fig. 1a, a certain volume of liquid is adsorbed in the corner of a truncated-cone-shaped container under microgravity. The blue region represents liquid with a volume of V_0. Figure 1b and c is enlarged cross-sectional views near the corner. The angle of the interior corner is α and the radius at the bottom of the container is r_0. φ is the angle between the z axis and the line in the direction normal to the profile. Points A and B are two endpoints of the profile, which are also located on walls of the container. When $\theta + \alpha > \pi/2$, the cross-section view of the liquid is shown in Fig. 1b. When $\theta + \alpha < \pi/2$, the cross-section view of the liquid is shown in Fig. 1c. In the second condition,

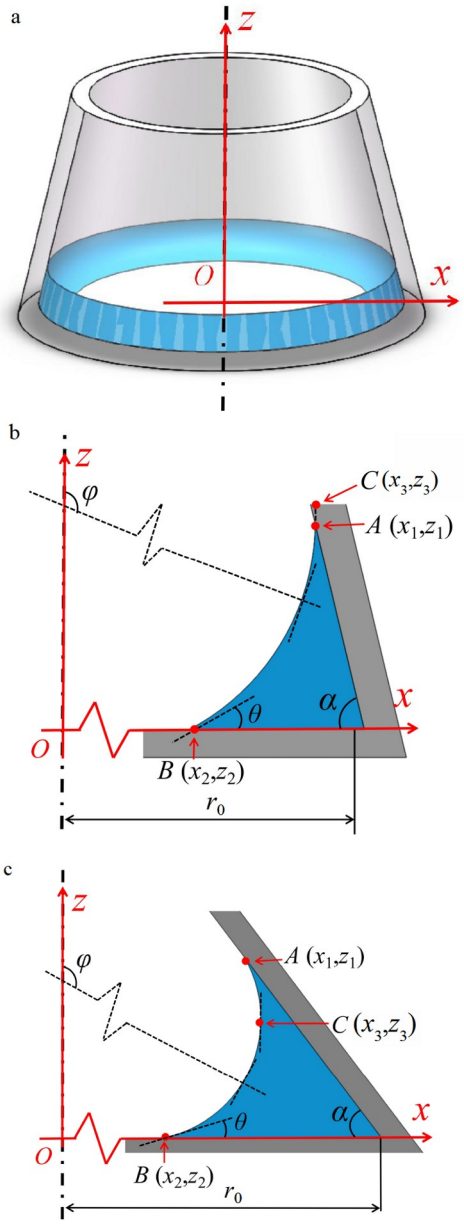

Figure 1 Schematic diagram of the model. **a** Front view of the whole model. **b** Cross-sectional view of the corner with $\theta + \alpha > \pi/2$. **c** Cross-sectional view of the corner with $\theta + \alpha < \pi/2$.

curve AB is divided into two segments, curve AC and curve BC, by point C, which is the point corresponding to $\varphi = \pi/2$. The contact angle of the liquid on container's wall is θ. The z axis is defined as the symmetry axis of the container, and the x axis is perpendicular to the z axis and is on the bottom of the container. Because the model is axisymmetric, the y axis is equivalent to the x axis and lies perpendicular to the plane of paper, and it is not shown in this study. In space, the gravity is less than $10^{-5}g$ (g is the gravity on the ground). In order to judge whether the gravity is negligible, we need to calculate the Bond number, which is the ratio of the gravity force to surface tension force. We take water as an example and the radius of the container in satellites is less than 1 m. The Bond number can be calculated to be less than 0.139. Actually, the radius is usually much smaller than 1 m, the Bond number will be much smaller than 1, and in this situation the effects of microgravity can be ignored. At each point on curve AB, there are two principal curvatures, K_1 and K_2.

Curvature K_1 in radial direction and curvature K_2 in azimuthal direction can be calculated as follows:

$$K_1 = -\frac{\mathrm{d}}{\mathrm{d}x}\frac{\mathrm{d}z/\mathrm{d}x}{\sqrt{1+(\mathrm{d}z/\mathrm{d}x)^2}}, \tag{1a}$$

$$K_2 = \frac{1}{x\sqrt{1+(\mathrm{d}z/\mathrm{d}x)^2}}. \tag{1b}$$

Adding up two curvatures leads to the capillary equation,

$$\frac{1}{x}\frac{\mathrm{d}}{\mathrm{d}x}\frac{x\mathrm{d}z/\mathrm{d}x}{\sqrt{1+(\mathrm{d}z/\mathrm{d}x)^2}} = C_1, \tag{2}$$

where C_1 is a constant. The expression $(\mathrm{d}z/\mathrm{d}x)/[1+(\mathrm{d}z/\mathrm{d}x)^2]^{0.5}$, radial component of the surface normal, equals the sine of surface's slope angle. After multiplying radius r, the first integral of Eq. (2) is obtained as

$$\frac{x\mathrm{d}z/\mathrm{d}x}{\sqrt{1+(\mathrm{d}z/\mathrm{d}x)^2}} = x\sin\varphi = \frac{C_1}{2}x^2 + C_2. \tag{3}$$

Combined with boundary conditions:

$$\begin{aligned} &x = x_1, \quad \varphi = \theta + \alpha, \\ &x = x_2, \quad \varphi = \pi - \theta, \\ &x = x_3, \quad \varphi = \pi/2. \end{aligned} \tag{4}$$

The constants can be obtained as follows:

for $\theta + \alpha > \pi/2$,

$$\begin{aligned} \text{curve } AB: \ C_1 &= 2\frac{x_1\sin(\theta+\alpha) - x_2\sin\theta}{x_1^2 - x_2^2}, \\ C_2 &= x_1x_2\frac{x_1\sin\theta - x_2\sin(\theta+\alpha)}{x_1^2 - x_2^2}, \end{aligned} \tag{5a}$$

for $\theta + \alpha < \pi/2$,

$$\begin{aligned} \text{curve } AC: \ C_1 &= 2\frac{x_1\sin(\theta+\alpha) - x_3}{x_1^2 - x_3^2}, \\ C_2 &= x_1x_3\frac{x_1 - x_3\sin(\theta+\alpha)}{x_1^2 - x_3^2}, \end{aligned} \tag{5b}$$

$$\begin{aligned} \text{curve } BC: \ C_1 &= 2\frac{x_2\sin\theta - x_3}{x_2^2 - x_3^2}, \\ C_2 &= x_2x_3\frac{x_2 - x_3\sin\theta}{x_2^2 - x_3^2}. \end{aligned} \tag{5c}$$

Using relationships:

for $\theta + \alpha > \pi/2$,

$$\text{curve } AB: \ -\frac{\mathrm{d}z}{\mathrm{d}x} = \tan\varphi = \frac{\sin\varphi}{-\left(1-\sin^2\varphi\right)^{0.5}}, \tag{6a}$$

for $\theta + \alpha < \pi/2$,

$$\text{curve } AC: \ -\frac{\mathrm{d}z}{\mathrm{d}x} = \tan\varphi = \frac{\sin\varphi}{\left(1-\sin^2\varphi\right)^{0.5}}, \tag{6b}$$

$$\text{curve } BC: \ -\frac{\mathrm{d}z}{\mathrm{d}x} = \tan\varphi = \frac{\sin\varphi}{-\left(1-\sin^2\varphi\right)^{0.5}} \tag{6c}$$

together with Eq. (3), allows the gradient of the profile, $\mathrm{d}z/\mathrm{d}x$, to be solved numerically by the Runge-Kutta method. Furthermore, Eqs. (6b) and (6c) can be expressed as a function of x, which can be simplified into expressions as follows:

$$\text{curve } AC: \ -\frac{\mathrm{d}z}{\mathrm{d}x} = \tan\varphi = \frac{\sin\varphi}{\left(1-\sin^2\varphi\right)^{0.5}} = \frac{x^2[x_1\sin(\theta+\alpha) - x_3] + x_1x_3[x_1 - x_3\sin(\theta+\alpha)]}{\left\{x^2[x_1\sin(\theta+\alpha) - x_3]^2\left(x_3^2 - x^2\right) - x_1^2[x_1 - x_3\sin(\theta+\alpha)]^2\left(x_3^2 - x^2\right)\right\}^{0.5}}. \tag{7a}$$

$$\text{curve } BC: \ -\frac{\mathrm{d}z}{\mathrm{d}x} = \tan\varphi = \frac{\sin\varphi}{-\left(1-\sin^2\varphi\right)^{0.5}} = \frac{x^2(x_2\sin\theta - x_3) + x_2x_3(x_2 - x_3\sin\theta)}{-\left[x^2(x_2\sin\theta - x_3)^2\left(x_3^2 - x^2\right) - x_2^2(x_2 - x_3\sin\theta)^2\left(x_3^2 - x^2\right)\right]^{0.5}}. \tag{7b}$$

Writing

$$\text{curve } AC: \ a_1 = \frac{x_1 - x_3\sin(\theta+\alpha)}{x_1\sin(\theta+\alpha) - x_3}, \tag{8a}$$

$$\text{curve } BC: \ a_2 = \frac{x_2 - x_3\sin\theta}{x_2\sin\theta - x_3}, \tag{8b}$$

Eqs. (7a) and (7b) can be written as

$$\text{curve } AC: \ -\frac{\mathrm{d}z}{\mathrm{d}x}=\frac{x^2+a_1x_1x_3}{\left[\left(x_3^2-x^2\right)\left(x^2-a_1^2x_1^2\right)\right]^{0.5}}, \tag{9a}$$

$$\text{curve } BC: \ \frac{\mathrm{d}z}{\mathrm{d}x}=\frac{x^2+a_2x_2x_3}{\left[\left(x_3^2-x^2\right)\left(x^2-a_2^2x_2^2\right)\right]^{0.5}}. \tag{9b}$$

Adopt variable substitutions,

$$\text{curve } AC: \ k_1^2=\frac{x_3^2-a_1^2x_1^2}{x_3^2}, \tag{10a}$$

$$\text{curve } BC: \ k_2^2=\frac{x_3^2-a_2^2x_2^2}{x_3^2}, \tag{10b}$$

$$\text{curve } AC: \ x^2=x_3^2\left(1-k_1^2\sin^2\phi\right), \tag{11a}$$

$$\text{curve } BC: \ x^2=x_3^2\left(1-k_2^2\sin^2\phi\right). \tag{11b}$$

This allows Eq. (9) to be integrated, which leads to

$$\text{curve } AC: \ z=-\left[a_1x_1F(\phi,k_1)+x_3E(\phi,k_1)\right]+C_3, \tag{12a}$$

$$\text{curve } BC: \ z=\left[a_2x_2F(\phi,k_2)+x_3E(\phi,k_2)\right]+C_4, \tag{12b}$$

where $F(\phi,k)$ and $E(\phi,k)$ are elliptic integrals of the first and second kind respectively, C_3 and C_4 are constants. Combined with points A and B, these two constants can be determined. This transformation simplifies the calculation process of the profile.

The volume of the liquid accumulated in corners is a matter of great concern. It is expressed as

$$V_0=V_A-V_{AB}, \text{ for } \theta+\alpha>\pi/2, \tag{13a}$$

$$V_0=V_A-V_{AC}-V_{BC}, \text{ for } \theta+\alpha<\pi/2, \tag{13b}$$

where V_0 is the liquid volume accumulated in corners, V_A is the volume of the container with a height of z_1 from the bottom, and V_{AB}, V_{AC} and V_{BC} are the volumes of gas surrounded by the liquid-gas interface.

The container's volume V_A is

$$V_A=\frac{\pi}{3}z_1\left(r_0^2+r_0x_1+x_1^2\right). \tag{14}$$

The volume of the solid of revolution is written as

$$V=\pi\int x^2\mathrm{d}z. \tag{15}$$

Combined with Eqs. (3)-(6) and (15), the volume of liquid accumulated in corners can be obtained.

Moreover, V_{AC} and V_{BC} can be changed into the form as follows:

$$V_{AC}=\pi\int_{z_3}^{z_1}x^2\mathrm{d}z=\frac{\pi x_3}{3}\left[\left(2a_1^2x_1^2+3a_1x_1x_3+2x_3^2\right)E(\phi_1,k_1)-a_1^2x_1^2F(\phi_1,k_1)+\frac{x_1}{x_3}\left(x_3^2-x_1^2\right)^{0.5}\left(x_1^2-a_1^2x_1^2\right)^{0.5}\right], \tag{16a}$$

$$V_{BC}=\pi\int_{z_2}^{z_3}x^2\mathrm{d}z=\frac{\pi x_3}{3}\left[\left(2a_2^2x_2^2+3a_2x_2x_3+2x_2^2\right)E(\phi_2,k_2)-a_2^2x_2^2F(\phi_2,k_2)+\frac{x_2}{x_3}\left(x_3^2-x_2^2\right)^{0.5}\left(x_2^2-a_2^2x_2^2\right)^{0.5}\right], \tag{16b}$$

which can simplify the calculation process. If the coordinates of points A, B and C are all known, the volume can be obtained according to Eqs. (13)-(16). The volume can also be obtained only based on x_2 using the shooting method. During this calculation process, x_1 and x_3 are decided using the shooting method and x_2 is the only independent variable.

3. Numerical simulation

To validate the proposed mathematical model, numerical simulation is performed with the VOF method. Figure 2 shows a typical mesh model of a truncated-cone-shaped container. Different sizes of containers are chosen. Grid-independent verification is carried out and the total number of grids is decided to be about 0.3 million. Boundary layers are established near all walls of the container. The flow is assumed to be laminar in our simulation. The time-step size is 0.0004 s and simulation results are saved automatically every 2000 steps. A kind of silicone oil named Shin-Etsu Company SF 2 is selected in this study. Its properties are listed in Table 1.

To save calculation time, liquid is initially accumulated in the corner. As shown in Fig. 3, the yellow surface stands for the liquid-gas interface, and the translucent blue surface is

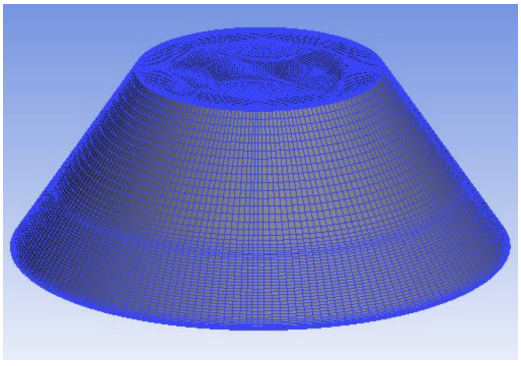

Figure 2 Mesh model established for numerical simulation.

Table 1 Liquid properties (25°C)

Liquid	μ (kg/(m s))	ρ (kg/m^3)	σ (N/m)	ν (10^{-6} m^2/s)
SF 2	0.001746	873	0.0183	2

Table 2 Model parameters and comparison between numerical and theoretical results

No.	Parameters			Numerical results						Theoretical predictions					Ratios of theoretical predictions to numerical results	
	r_0 (mm)	α (°)	θ (°)	x_1 (mm)	z_1 (mm)	x_2 (mm)	x_3 (mm)	z_3 (mm)	V_0 (mm^3)	x_1 (mm)	z_1 (mm)	x_3 (mm)	z_3 (mm)	V_0 (mm^3)	Ratios of z_1 (%)	Ratios of V_0 (%)
#1	20	90	30	20	10.33	9.317	–	–	5058	20	10.45	–	–	4828	101.2	95.45
#2	20	90	40	20	10.68	7.693	–	–	6771	20	11.09	–	–	6390	103.8	94.37
#3	20	90	50	20	8.690	10.40	–	–	5058	20	8.816	–	–	4674	101.5	92.41
#4	20	108.4	20	23.78	11.43	8.250	–	–	5426	23.61	10.84	–	–	5218	94.84	96.17
#5	20	108.4	30	23.22	9.744	7.681	–	–	6387	23.43	10.32	–	–	6103	105.9	95.55
#6	20	108.4	40	23.10	9.379	8.252	–	–	6387	23.08	9.248	–	–	6077	98.60	95.15
#7	20	108.4	50	22.15	6.916	12.24	–	–	3944	22.16	6.502	–	–	3478	94.01	88.18
#8	40	45	15	28.06	11.83	22.86	29.11	7.681	16286	27.63	12.37	28.78	8.054	15146	104.6	93.00
#9	40	45	60	30.31	9.64	26.07	–	–	13977	30.16	9.841	–	–	13374	102.1	95.69
#10	40	56.31	20	30.12	14.85	21.27	30.91	10.91	19242	29.38	15.93	29.78	12.60	21347	107.3	110.9
#11	40	56.31	50	34.90	7.558	30.66	–	–	7830	34.81	7.787	–	–	7476	103.0	95.48
#12	40	56.31	60	35.52	6.694	31.53	–	–	7353	35.31	7.037	–	–	6596	105.1	89.70
#13	60	39.81	30	41.11	15.63	34.59	41.63	11.31	47242	40.29	16.43	41.14	11.64	49885	105.1	105.6
#14	60	39.81	60	49.34	8.792	45.83	–	–	19193	49.11	9.078	–	–	20051	103.3	104.5
#15	60	101.3	30	63.00	15.12	44.23	–	–	39416	63.10	15.51	–	–	37348	102.6	94.75
#16	60	101.3	40	62.88	14.56	44.71	–	–	39416	62.93	14.69	–	–	39736	100.9	100.8
#17	80	26.57	35	57.19	11.23	54.16	58.13	6.467	54079	56.83	11.59	57.91	7.296	53378	103.2	98.70
#18	80	26.57	65	59.46	10.18	56.92	–	–	51175	59.35	10.33	–	–	47585	101.5	92.98
#19	80	69.44	30	72.26	20.52	57.80	–	–	85320	72.09	21.10	–	–	82781	102.8	97.02
#20	80	69.44	50	72.93	18.57	59.64	–	–	85320	72.87	19.02	–	–	82719	102.4	96.95

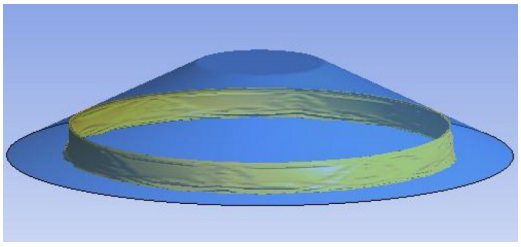

Figure 3 Initial liquid-gas interface in a container.

container's wall. The volume of the liquid accumulated in the corner and the contact angle of the liquid on container's wall are given, and they are also listed in Table 2. The container is high enough to prevent the liquid from reaching the top. There are two cases, one is that the amount of liquid is not enough and it forms a liquid drop somewhere in the corner instead of covering the entire circle of the corner; the other one is that the amount of liquid is too much and it covers the entire bottom of containers, which are not discussed in this paper.

The numerical calculation time is long enough for the liquid to reach equilibrium. The free interface at equilibrium is shown in Fig. 4a and the cross-sectional view of static liquid distribution in the corner is shown in Fig. 4b. In Fig. 4a, it can be seen that, when $\theta + \alpha \geq \pi/2$, there is no point on the profile such that the tangent at this point is perpendicular to the x-axis, therefore, the profile is curve AB as shown in the theoretical analysis. In Fig. 4b, when $\theta + \alpha < \pi/2$, there exists a point on the profile such that the tangent at this point is perpendicular to the x-axis, and this is point C. To compare with theoretical results, final results are obtained by reading two sets of coordinate values of points A, B and C on two cross-sectional profiles at two different moments from simulation results, and taking average of the two sets of coordinate values for points A, B and C respectively. Result data are listed in Table 2.

4. Results and discussions

In the simulation, the geometry of containers and the volume and contact angle of the liquid are all given. And the coordinates of points A, B and C can be measured. These numerical results can be compared with theoretical predictions to verify the mathematical model. Theoretical predictions are based on certain inputs. Two situations are discussed in this paper. The first situation is that the container's geometry, the liquid contact angle and the value of x_2 are used as inputs. While the second situation is that the container's geometry, the liquid contact angle and the volume of liquid are used as inputs.

In the first situation, theoretical predictions of the profile and volume of the liquid can be obtained by inserting x_2 into the mathematical model. When $\theta + \alpha > \pi/2$, x_2 measured from numerical results is substituted into the mathematical model proposed above, then x_1 is adjusted in a given range

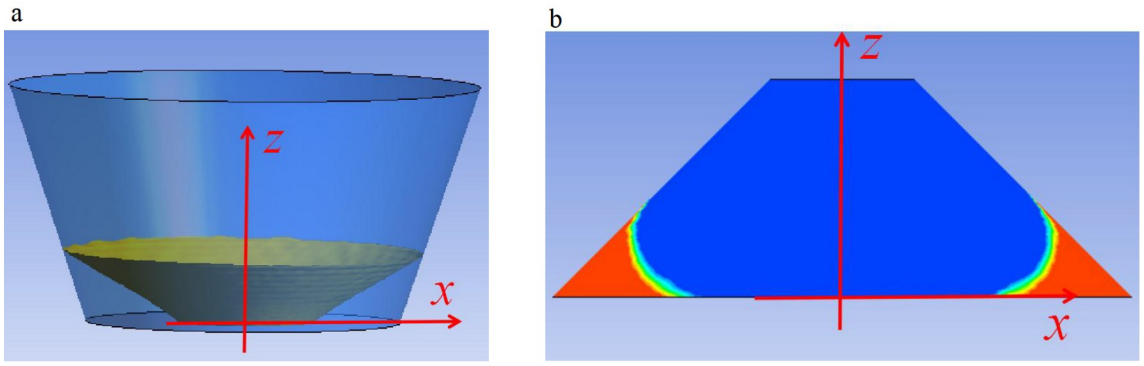

Figure 4 Distribution of SF 2 at equilibrium. **a** r_0 = 20 mm, α = 108.4°, θ = 40°. **b** r_0 = 40 mm, α = 45°, θ = 15°.

using the shooting method until it is on the container's wall. Once x_1 is determined, theoretical predictions of the profile and volume of the liquid will also be obtained. When $\theta + \alpha < \pi/2$, the calculation process is similar to that proposed above, and both x_1 and x_3 are adjusted until x_1 is on the container's wall.

Theoretical values of x_1, z_1, x_3, z_3 and V_0 are shown in Table 2. The ratios of theoretical predictions to numerical results are also given in the table. Points A and B are located on the wall. Their locations are easy to identify and relatively easy to measure. When $\theta + \alpha < \pi/2$, the coordinates of point C need to be measured from numerical results, and the measurement of the position of point C is dependent on the subjective judgement, which may cause a little error. Generally speaking, theoretical and numerical results are very close in z_1 and V_0, and the error is acceptable. In our simulation, the volume of liquid is given at first so that we can compare the given volume with the predicted results. In fact, the volume of liquid accumulated in the corner is hard to measure directly in the simulation if the volume is not given at first. But the coordinates of x_2 can be easily measured. Once x_2 is obtained, according to the mathematical model, the volume of liquid accumulated in the corner can be calculated.

To compare numerical and theoretical results of the profile more comprehensively, we measure coordinates of several points on the profile under different conditions from numerical results, and plot the points together with theoretical curves, as shown in Fig. 5. The case numbers are labeled in the upper-left corner of the figure. In cases 1, 16 and 19, $\theta + \alpha > \pi/2$, while in cases 8 and 17, $\theta + \alpha < \pi/2$. And the value of r_0 varies from 20 mm to 80 mm while the value of α varies from 26.57° to 101.3°. The solid curves are theoretical results and the squares represent the points taken from numerical results. Different colors represent different conditions, which are annotated in the upper left corner of the figure. The profiles from numerical results are in good agreement with those from theoretical results.

In the second situation, the abscissa values of points A, B and C are unknown, but the volume of liquid is given as an input. When $\theta + \alpha > \pi/2$, the volume of liquid V_0 is considered to be a function of x_2, and it can be obtained using the dichotomy method. Firstly, x_2 is estimated within a given range, and then the values of liquid volume are calculated based on different values of x_2 until the deviation from the given volume of liquid is less than 0.01%. Once x_2 is determined, the profile can be obtained using the shooting method. When $\theta + \alpha < \pi/2$, the calculation process is similar to that proposed above. x_2 is obtained using the dichotomy method at first. Then we adjust both x_1 and x_3 using the shooting method until x_1 locates on the container's wall. By using the values of r_0, α, θ and V_0 in Table 2, theoretical predictions of coordinates of points A, B and C are obtained and ratios of predicted to numerical results are shown in Table 3.

To observe the accuracy of theoretical predictions, ratios of theoretical to numerical results are shown in Fig. 6a and b. The abscissa represents the case number, and the ordinate represents the ratio. Figure 6a shows ratios when x_2 is given and Fig. 6b shows ratios when V_0 is given. It can be seen that, in most cases, the ratios are within 100% ± 5%. And the maximum deviation is also within ±12%. It indicates that theoretical predictions based on the mathematical model using the shooting method are in good agreement with numerical results.

The numerical method proposed above has important applications in spacecraft or orbiting vehicles. For example, it can be useful in many applications associated with utilization of propellant in tanks. Firstly, simulate the process of propellant extrusion under microgravity. When the propellant stops flowing out of the tank, there must be some residual in corners. And the volume of residual is hard to measure from the numerical results. But the container's geometry and liquid contact angle are known, and x_2 can be easily measured from numerical results. Based on these inputs, the volume of propellant absorbed in corners can be calculated. Our numerical method will be helpful for calculating the utilization of propellant. Compared with

Table 3 Predicted values compared with numerical results

No.	Theoretical predictions					Ratios of predicted to numerical results		
	x_1 (mm)	z_1 (mm)	x_2 (mm)	x_3 (mm)	z_3 (mm)	Ratios of x_1 (%)	Ratios of x_2 (%)	Ratios of x_3 (%)
#1	20	10.70	9.007	–	–	100	96.67	–
#2	20	11.41	7.139	–	–	100	92.80	–
#3	20	9.174	9.901	–	–	100	95.20	–
#4	23.68	11.05	7.954	–	–	99.58	96.41	–
#5	23.51	10.54	7.248	–	–	101.2	94.36	–
#6	23.14	9.448	7.776	–	–	100.2	94.23	–
#7	22.30	6.903	11.62	–	–	100.7	94.93	–
#8	27.10	12.90	22.14	28.30	8.398	96.58	96.85	97.22
#9	29.91	10.09	25.71	–	–	98.68	98.62	–
#10	30.00	15.00	22.43	30.37	11.87	99.60	105.5	98.25
#11	34.68	7.982	30.43	–	–	99.37	99.25	–
#12	35.03	7.456	31.02	–	–	98.62	98.38	–
#13	40.91	15.91	35.38	41.73	11.28	99.51	102.3	100.2
#14	49.36	8.867	46.16	–	–	100.4	100.7	–
#15	63.19	15.94	43.78	–	–	100.3	98.98	–
#16	62.92	14.63	44.78	–	–	100.1	100.2	–
#17	56.66	11.67	53.97	57.75	7.350	99.07	99.65	99.35
#18	58.49	10.76	55.96	–	–	98.37	98.31	–
#19	71.96	21.45	57.44	–	–	99.58	99.38	–
#20	72.75	19.33	59.30	–	–	99.75	99.43	–

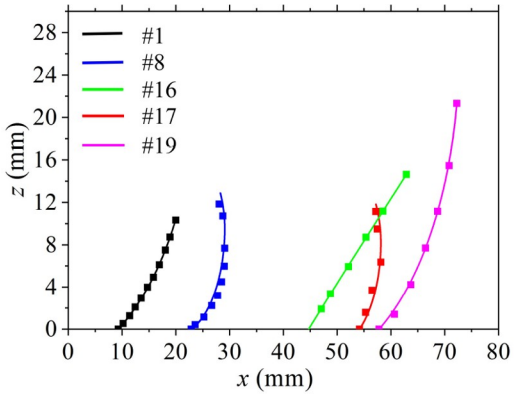

Figure 5 Comparison between theoretical and numerical results.

surface evolve or fluent, our method is much easier and needs much less work to obtain the profiles and volume of liquid absorbed in the corner. Besides, the method based on the Gibbs free energy proposed before is more complicated than ours. The previous method needs a series of equations to describe the Gibbs free energy of the free surface. And solve the equations to obtain the minimum of the Gibbs free energy to further predict the profile. Our method uses the geometry of the container as the boundary condition, which is much easier than the previous method.

Predicted profiles are shown in Fig. 7a when $\theta + \alpha > \pi/2$ and Fig. 7b when $\theta + \alpha < \pi/2$. The black lines represent the profile of the container's wall and the colored curves stand for profiles of the liquid under different conditions. The profiles are similar to those in Figs. 4a and b. When $\theta + \alpha < \pi/2$, the profile of the liquid is divided into two sections and there exists a point where the tangent line is perpendicular to the x-axis.

For further analysis, dimensionless expressions of profiles are given as follows:

$$\text{curve } AB: \quad \frac{\mathrm{d}\bar{z}}{\mathrm{d}\bar{x}} = \tan\varphi = \frac{\sin\varphi}{\left(1-\sin^2\varphi\right)^{0.5}},$$
$$\bar{C}_1 = 2\frac{\bar{x}_1\sin(\theta+\alpha)-\bar{x}_2\sin\theta}{\bar{x}_1^2-\bar{x}_2^2}, \tag{17a}$$
$$\bar{C}_2 = \bar{x}_1\bar{x}_2\frac{\bar{x}_1\sin\theta-\bar{x}_2\sin(\theta+\alpha)}{\bar{x}_1^2-\bar{x}_2^2},$$

$$\text{curve } AC: \quad -\frac{\mathrm{d}\bar{z}}{\mathrm{d}\bar{x}} = \frac{\bar{x}^2+\bar{a}_1\bar{x}_1\bar{x}_3}{\left[\left(\bar{x}_3^2-\bar{x}^2\right)\left(\bar{x}^2-\bar{a}_1^2\bar{x}_1^2\right)\right]^{0.5}}, \tag{17b}$$
$$\bar{a}_1 = \frac{\bar{x}_1-\bar{x}_3\sin(\theta+\alpha)}{\bar{x}_1\sin(\theta+\alpha)-\bar{x}_3},$$

$$\text{curve } BC: \quad \frac{\mathrm{d}\bar{z}}{\mathrm{d}\bar{x}} = \frac{\bar{x}^2+\bar{a}_2\bar{x}_2\bar{x}_3}{\left[\left(\bar{x}_3^2-\bar{x}^2\right)\left(\bar{x}^2-\bar{a}_2^2\bar{x}_2^2\right)\right]^{0.5}}, \tag{17c}$$
$$\bar{a}_2 = \frac{\bar{x}_2-\bar{x}_3\sin\theta}{\bar{x}_2\sin\theta-\bar{x}_3},$$

$$\bar{V}_A = \frac{\pi}{3}\bar{z}_1\left(1+\bar{x}_1+\bar{x}_1^2\right), \tag{18}$$

$$\bar{V} = \pi\int\bar{x}^2\mathrm{d}\bar{z}, \tag{19}$$

where $\bar{x}_1 = x_1/r_0$, $\bar{x}_2 = x_2/r_0$, $\bar{x}_3 = x_3/r_0$, $\bar{z}_1 = z_1/r_0$,

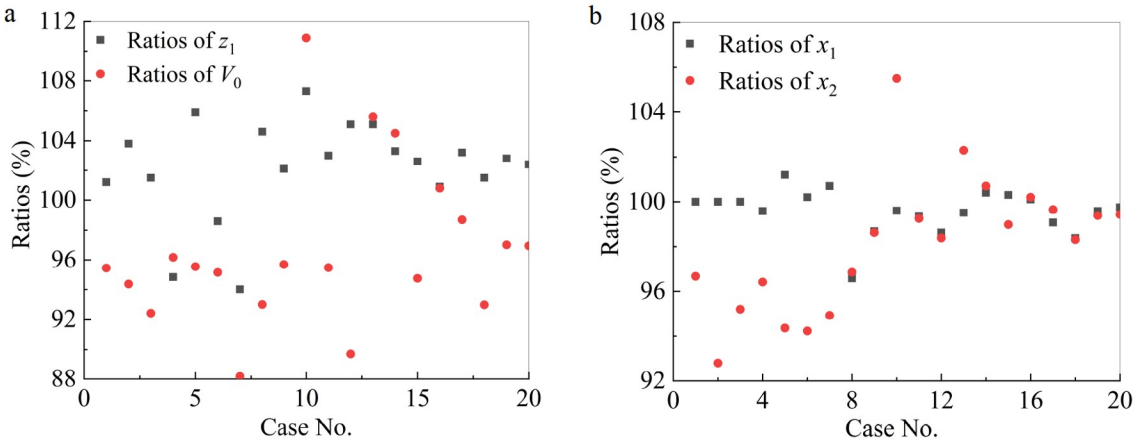

Figure 6 Ratios of theoretical predictions to numerical results. **a** Ratios when x_2 is given and **b** ratios when V_0 is given.

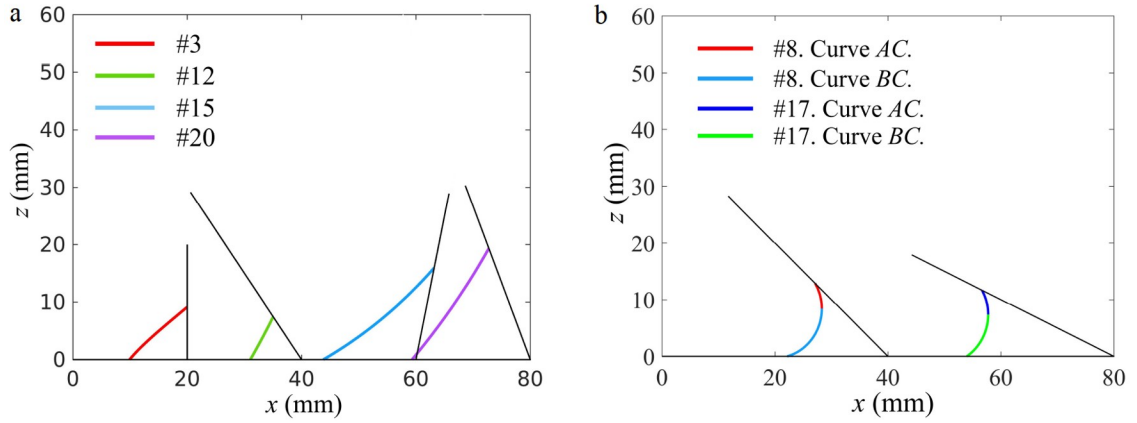

Figure 7 Predicted profiles based on the dichotomy method and shooting method. **a** $\theta + \alpha > \pi/2$. **b** $\theta + \alpha < \pi/2$.

$\bar{x} = x / r_0$ and $\bar{z} = z / r_0$.

Changes of dimensionless liquid volume with contact angle of the liquid or the angle of the corner are shown in Fig. 8a-d respectively. The abscissa represents contact angle or angle of the corner, and the ordinate represents the dimensionless volume. The figures show changes of liquid volume when $\bar{x}_2 = 0.5$, 0.6 and 0.7. It can be seen that liquid volume always increases monotonously with increase of the contact angle or the angle of the corner. For a wide range of abscissa values, α is set to be 71° in Fig. 8a but 29° in Fig. 8c, and θ is set to be 80° in Fig. 8b but 30° in Fig. 8d. Comparing the changes of the volume of liquid at different values of $\bar{x}_2$, it can be seen that the volume of liquid increases at a higher rate with the increase of the liquid contact angle or the angle of the corner when $\bar{x}_2$ is smaller.

5. Conclusions

Understanding capillary phenomena in the corner of truncated-cone-shaped containers under microgravity is important because it will be helpful for liquid management in space. The mathematical model of the profile of the liquid accumulated in the corner is derived. According to liquid's wettability and the angle of the container's corner, the profiles have two cases: when $\theta + \alpha < \pi/2$, there exists a point named point C such that the tangent at this point is perpendicular to the x-axis; when $\theta + \alpha > \pi/2$, there is no point C on the profile. Numerical simulation is performed with the VOF method and numerical results are consistent with theoretical predictions.

Based on the model, expressions of liquid volume are also obtained. As the geometry of containers and the contact angle of the liquid are given, if one of abscissa values of points A, B and C is known, theoretical predictions of the profile and volume of the liquid can be obtained using the shooting method; if abscissa values of points A, B and C are unknown, the profile of the liquid at equilibrium can also be obtained using the dichotomy method and shooting method if liquid volume V_0 is known. These methods are easier than the method based on the Gibbs free energy discussed before,

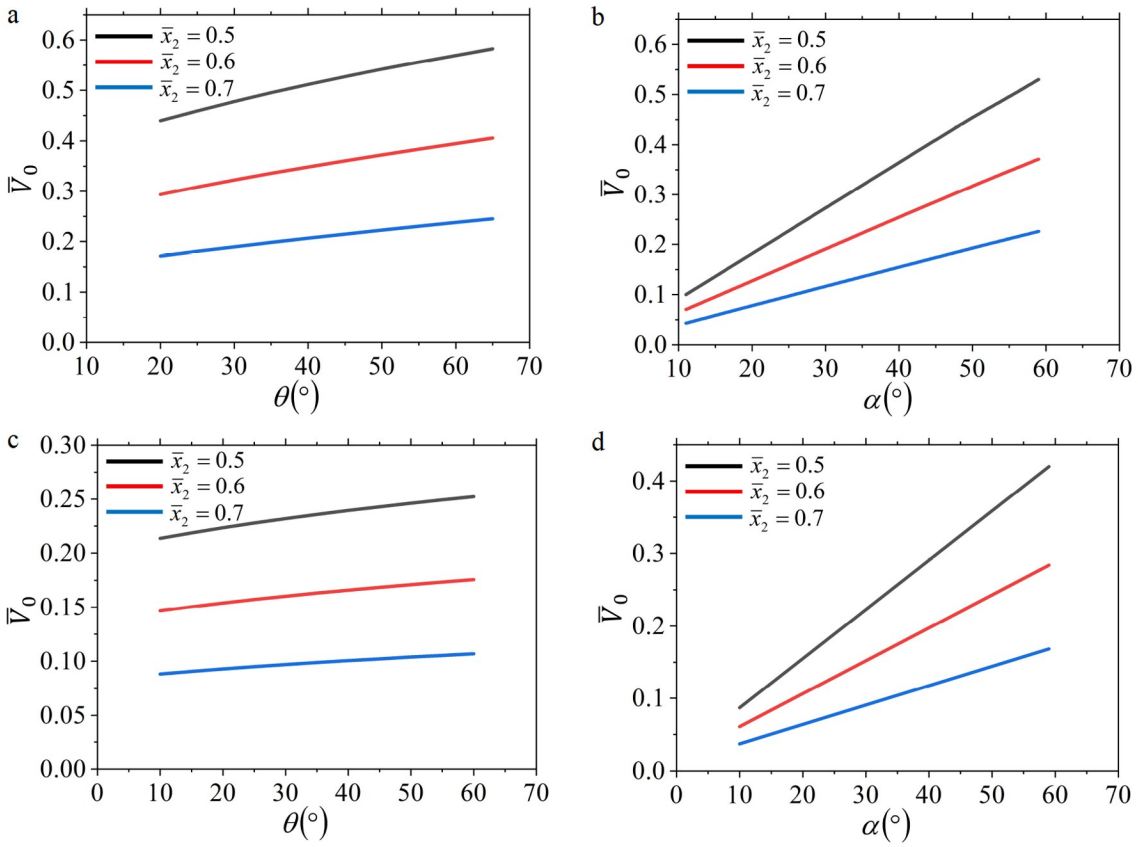

Figure 8 Changes of dimensionless liquid volume. **a** Volume vs. the contact angle when α = 71°. **b** Volume vs. the angle of the corner when θ = 80°. **c** Volume vs. the contact angle when α = 29°. **d** Volume vs. the angle of the corner when θ = 30°.

and can also be used to predict profiles of the liquid in other situations, such as liquid bridges between two different spheres. Based on the mathematical expressions presented in this study, the profile and volume of the liquid accumulated in the corner of truncated-cone-shaped containers can be predicted accurately. The numerical methods proposed in this paper have important applications in aerospace. For example, it can be used to calculate the utilization of propellant in tanks.

Author contributions *Shangtong Chen designed the research. Shangtong Chen and Chu Zhang wrote the first draft of the manuscript. Shangtong Chen and Chu Zhang set up the numerical set-up and processed the numerical data. Wen Li, Yong Li and Fenglin Ding helped organize the manuscript. Wen Li, Yong Li and Qi Kang revised and edited the final version.*

Acknowledgements *This work was supported by the China Manned Space Engineering Program (Fluid Physics Experimental Rack and the Priority Research Program of Space Station), and the National Natural Science Foundation of China (Grant No. 12032020).*

1 R. Lucas, Rate of capillary ascension of liquids, Kolloid-Zeitschrift **23**, 15 (1918).
2 E. W. Washburn, The dynamics of capillary flow, Phys. Rev. **17**, 273 (1921).
3 S. Levine, P. Reed, E. J. Watson, and G. Neale, A theory of the rate of rise of a liquid in a capillary, J. Colloid Interface Sci. **3**, 403 (1976).
4 M. Stange, M. E. Dreyer, and H. J. Rath, Capillary driven flow in circular cylindrical tubes, Phys. Fluids **15**, 2587 (2003).
5 S. Chen, Z. Ye, L. Duan, and Q. Kang, Capillary driven flow in oval tubes under microgravity, Phys. Fluids **33**, 032111 (2021).
6 J. Lei, Z. Xu, F. Xin, and T. J. Lu, Dynamics of capillary flow in an undulated tube, Phys. Fluids **33**, 052109 (2021).
7 B. Figliuzzi, and C. R. Buie, Rise in optimized capillary channels, J. Fluid Mech. **731**, 142 (2013).
8 S. Chen, Y. Chen, L. Duan, and Q. Kang, Capillary rise of liquid in concentric annuli under microgravity, Microgravity Sci. Technol. **34**, 30 (2022).
9 R. Chassagne, F. Dörfler, M. Guyenot, and J. Harting, Modeling of capillary-driven flows in axisymmetric geometries, Comput. Fluids **178**, 132 (2019).
10 D. A. Bolleddula, Y. Chen, B. Semerjian, N. Tavan, and M. M. Weislogel, Compound capillary flows in complex containers: Drop tower test results, Microgravity Sci. Technol. **22**, 475 (2010).
11 X. Wang, Y. Pang, Y. Ma, Y. Ren, and Z. Liu, Flow regimes of the immiscible liquids within a rectangular microchannel, Acta Mech. Sin. **37**, 1544 (2021).
12 C. E. Wu, J. Qin, and P. Gao, Experiment on gas-liquid displacement in a capillary, Acta Mech. Sin. **38**, 321386 (2022).
13 M. Dreyer, A. Delgado, and H. J. Path, Capillary rise of liquid between parallel plates under microgravity, J. Colloid Interface Sci. **163**, 158 (1994).
14 S. Chen, L. Duan, Y. Li, F. Ding, J. Liu, and W. Li, Capillary phenomena between plates from statics to dynamics under microgravity, Microgravity Sci. Technol. **34**, 70 (2022).
15 T. S. Ramakrishnan, P. Wu, H. Zhang, and D. T. Wasan, Dynamics in closed and open capillaries, J. Fluid Mech. **872**, 5 (2019).

16 M. M. Weislogel, and S. Lichter, Capillary flow in an interior corner, J. Fluid Mech. **373**, 349 (1998).
17 M. M. Weislogel, and C. L. Nardin, Capillary driven flow along interior corners formed by planar walls of varying wettability, Microgravity Sci. Technol **17**, 45 (2005).
18 Y. Chen, M. M. Weislogel, and C. L. Nardin, Capillary-driven flows along rounded interior corners, J. Fluid Mech. **566**, 235 (2006).
19 Y. Li, M. Hu, L. Liu, Y. Y. Su, L. Duan, and Q. Kang, Study of capillary driven flow in an interior corner of rounded wall under microgravity, Microgravity Sci. Technol. **27**, 193 (2015).
20 Z. Wu, Y. Huang, X. Chen, and X. Zhang, Capillary-driven flows along curved interior corners, Int. J. Multiphase Flow **109**, 14 (2018).
21 Y. Tian, Y. Jiang, J. Zhou, and M. Doi, Dynamics of Taylor rising, Langmuir **35**, 5183 (2019).
22 J. Zhou, and M. Doi, Universality of capillary rising in corners, J. Fluid Mech. **900**, A29 (2020).
23 M. M. Weislogel, and J. T. McCraney, The symmetric draining of capillary liquids from containers with interior corners, J. Fluid Mech. **859**, 902 (2018).
24 S. Chen, Z. Han, L. Duan, and Q. Kang, Experimental and numerical study on capillary flow along deflectors in plate surface tension tanks in microgravity environment, AIP Adv. **9**, 025020 (2019).
25 S. Chen, L. Duan, and Q. Kang, Study on propellant management device in plate surface tension tanks, Acta Mech. Sin. **37**, 1498 (2021).
26 P. Concus, and R. Finn, On capillary free surfaces in the absence of gravity, Acta Math. **132**, 177 (1974).
27 B. J. Carroll, The accurate measurement of contact angle, phase contact areas, drop volume, and Laplace excess pressure in drop-on-fiber systems, J. Colloid Interface Sci. **57**, 488 (1976).
28 S. Michielsen, J. Zhang, J. Du, and H. J. Lee, Gibbs free energy of liquid drops on conical fibers, Langmuir **27**, 11867 (2011).
29 J. Du, S. Michielsen, and H. J. Lee, Profiles of liquid drops at the tips of cylindrical fibers, Langmuir **26**, 16000 (2010).
30 J. Du, S. Michielsen, and H. J. Lee, Profiles of liquid drops at the bottom of cylindrical fibers standing on flat substrates, Langmuir **28**, 722 (2011).
31 G. Mason, and W. C. Clark, Liquid bridges between spheres, Chem. Eng. Sci. **20**, 859 (1965).
32 W. C. Clark, J. M. Haynes, and G. Mason, Liquid bridges between a sphere and a plane, Chem. Eng. Sci. **23**, 810 (1968).
33 M. A. Fortes, Axisymmetric liquid bridges between parallel plates, J. Colloid Interface Sci. **88**, 338 (1982).
34 J. W. van Honschoten, N. R. Tas, and M. Elwenspoek, The profile of a capillary liquid bridge between solid surfaces, Am. J. Phys. **78**, 277 (2010).
35 Y. Wang, S. Michielsen, and H. J. Lee, Symmetric and asymmetric capillary bridges between a rough surface and a parallel surface, Langmuir **29**, 11028 (2013).
36 T. P. Farmer, and J. C. Bird, Asymmetric capillary bridges between contacting spheres, J. Colloid Interface Sci. **454**, 192 (2015).
37 E. Reyssat, Capillary bridges between a plane and a cylindrical wall, J. Fluid Mech. **773**, R1 (2015).
38 H. D. Mittelmann, Symmetric capillary surface in a cube, Math. Comput. Simul. **35**, 139 (1993).
39 D. Langbein, Liquid surfaces in polyhedral containers, in: Capillary Surfaces (Springer, Berlin, Heidelberg, 2002), pp. 213-234.
40 J. B. Bostwick, and P. H. Steen, Stability of constrained capillary surfaces, Annu. Rev. Fluid Mech. **47**, 539 (2015).
41 J. Zou, F. Lin, and C. Ji, Capillary breakup of armored liquid filaments, Phys. Fluids **29**, 062103 (2017).

微重力下圆台形容器内角处毛细现象

陈上通, 章楚, 李文, 李永, 丁凤林, 康琦

摘要 在微重力环境中, 液体通常吸附在夹角或缝隙中. 积聚在这些区域的液体难以排出和使用. 本文通过理论推导得到了微重力环境下圆台形容器内角处液体的气液界面轮廓. 根据液体的润湿性和内角大小, 界面轮廓可分为两种情况. 一旦知道轮廓某个端点的坐标, 就可以根据数学模型使用打靶法获得液面轮廓和体积. 此外, 如果轮廓端点的横坐标值无法测量得到, 在给定液体体积的情况下, 也可以使用二分法和打靶法获得液面轮廓. 本文提出的方法比之前提出的基于Gibbs自由能的方法更容易. 该方法也可用来预测其他结构间的液面轮廓. 本文采用有限体积法开展数值模拟, 仿真结果与理论值吻合良好. 基于该数学模型, 可准确预测圆台形容器内角处积聚液体的液面轮廓和体积.